Role of Electrochemically Driven Cu Nanograins in $CuGa_2$ Electrode

Kyu T. Lee,† Yoon S. Jung, Ji Y. Kwon, Jun H. Kim, and Seung M. Oh*

Department of Chemical and Biological Engineering and Research Center for Energy Conversion & Storage, Seoul National University, San56-1 Shillim-dong, Gwanak-gu, Seoul, 151-744, Korea

Received August 3, 2007. Revised Manuscript Received November 13, 2007

Upon lithiation, the active (Ga) and inactive component (Cu) in a binary intermetallic $CuGa_2$ electrode are converted to nanograins (<50 nm) of Li_xGa and metallic Cu, respectively. It was found that the Cu nanograins are not idling as an inactive ingredient but have a strong influence on the thermodynamic and kinetic properties of Li_xGa phases through a partial bonding to Ga atoms of Li_xGa (Cu→Ga−Li). The Li_xGa phase diagram is altered by the presence of Cu nanograins, eloquently demonstrating that the surface energy becomes more important than internal energy in controlling thermodynamics of nanosized materials. The lithiation rate is slower than that for pure Ga electrode because of activation energy needed for bond cleavage of the partial bonding. The delithiation rate capability is, however, exceptionally good; the capacity at 26 *C* amounts to 91% of that at 0.13 *C*, which is indebted to a weakening in the Ga−Li bond by the Cu→Ga partial bonding.

Introduction

In recent years, the issues of environmental pollution and exhaustion of natural energy drive a continuous development of cleaner, more fuel-efficient hybrid electric vehicles (HEV), wherein lithium ion batteries (LIB) with their superior performance to nickel−metal hydride cells are now being considered as the future power source for HEV. One of the major challenges with LIB for HEV application is, among others, the development of new electrode materials that charge–discharge at high rates. To this end, many nanosized electrode materials and their preparation methods have been developed: nanosized powder electrodes,[1–3] thin film electrodes of nanometer thickness,[4] and nanostructured electrodes having columnar structure or porous structures.[5–9] In all these efforts, the underlying strategy is the shortening of Li^+ diffusion paths. Such a nanosized approach, however, still possesses problems: high irreversible capacity caused by large surface area and potentially more complex synthesis than that for bulkier materials. Even further, the environmental, health, and safety issues for nanosized materials have not been cleared yet. Here we present other types of negative electrode materials that discharge at high rates, which are the binary intermetallic compounds (A_xB_y) comprising active A and inactive B atom. The key feature in achieving high rates in these electrodes is different from the conventional ones: weakening the Li−A bond by a strong interaction exerted by the inactive B component, which allows a high delithiation rate. This approach seems to be still within the regime of nanosized strategy because both the lithiated active A component (Li−A) and inactive B carry a nanostructure but differs from the conventional ones in that the nanostructures are in situ generated from film or micron-sized powder electrodes during the electrochemical lithiation period.

Binary intermetallic compounds have been projected as the negative electrode for lithium ion batteries as a way to solve or at least alleviate the intrinsic problems encountered in pure Li alloy materials (Si,[10,11] Sn,[12,13] and Sb[13,14]), which show a poor cycle performance due to electrode degradation caused by repeated volume change. In this approach, an inactive component (B) has been incorporated into the active alloy material (A = Si, Sn, and Sb) with an expectation that the inactive B plays a buffering role against the volume change associated with active A. As a matter of fact, several reports claimed a much improved cycle performance with this approach: Cu_6Sn_5,[15,16] $Co_{1-x}Sn_x$,[17] Ni_xSn,[18] $CoSb_3$,[19] and $CuSb_2$.[20] As far as the authors know, however, additional

* Corresponding author. E-mail: seungoh@snu.ac.kr.
† Present address: Department of Chemistry, University of Waterloo, Ontario, Canada N2L3G1.

(1) Hu, Y. S.; Kienle, L.; Guo, Y. G.; Maier, J. *Adv. Mater.* **2006**, *18*, 1421.
(2) Armstrong, G.; Armstrong, A. R.; Bruce, P. G.; Scrosati, B *Adv. Mater.* **2006**, *18*, 2597.
(3) Okubo, M.; Hosono, E.; Kim, J.; Enomoto, M.; Kojima, N.; Kudo, T.; Zhou, H.; Honma, I. *J. Am. Chem. Soc.* **2007**, *129*, 7444.
(4) Graetz, J.; Ahn, C. C.; Yazami, R.; Fultz, B. *J. Electrochem. Soc.* **2004**, *151*, A698.
(5) Taberna, P. L.; Mitra, S.; Poizot, P.; Simon, P.; Tarascon, J. M. *Nat. Mater.* **2006**, *5*, 567.
(6) Li, N.; Martin, C. R.; Scrosati, B. A. *Electrochem. Solid-State Lett.* **2000**, *3*, 316.
(7) Ergang, N. S.; Lytle, J. C.; Lee, K. T.; Oh, S. M.; Smyrl, W. H.; Stein, A. *Adv. Mater.* **2006**, *18*, 1750.
(8) Lee, K. T.; Lytle, J. C.; Ergang, N. S.; Oh, S. M.; Stein, A. *Adv. Funct. Mater.* **2005**, *15*, 547.
(9) Sorensen, E. M.; Barry, S. J.; Jung, H. K.; Rondinelli, J. R.; Vaughey, J. T.; Poeppelmeier, K. R. *Chem. Mater.* **2006**, *18*, 482.
(10) Obrovac, M. N.; Christensen, L. *Electrochem. Solid-State Lett.* **2004**, *7*, A93.
(11) Hatchard, T. D.; Dahn, J. R. *J. Electrochem. Soc.* **2004**, *151*, A838.
(12) Lee, K. T.; Jung, Y. S.; Oh, S. M. *J. Am. Chem. Soc.* **2003**, *125*, 5652.
(13) Yang, J.; Wachtler, M.; Winter, M.; Besenhard, J. O. *Electrochem. Solid-State Lett.* **1999**, *2*, 161.
(14) Vaughey, J. T.; Johnson, C. S.; Kropf, A. J.; Benedek, R.; Thackeray, M. M.; Tostmann, H.; Sarakonsri, T.; Hackney, S.; Fransson, L.; Edstrom, K.; Thomas, J. O. *J. Power Sources* **2001**, *97–98*, 194.

10.1021/cm702181m CCC: $40.75
Published on Web 12/22/2007

roles of the inactive component except for the buffering action against volume change have not been reported in the literature. In addition, literature survey finds that some of binary intermetallic electrodes are inactive for lithiation at room temperature even though the reaction is thermodynamically feasible.[21,22] Intuitively, such a slow kinetics can be attributed to a high activation energy needed for bond dissociation between A−B.[16,21,23] The kinetic aspects of these inactive intermetallic compounds have not, however, been fully characterized as far as the authors know.

The following goals have been identified in this work: (i) variable temperature (25–120 °C) study on binary intermetallic electrodes to examine their lithiation/delithiation kinetics, (ii) trace of morphological change of active and inactive component with Li^+ uptake/extraction, and (iii) extraction of the role of inactive component B in affecting the kinetic and thermodynamic behavior of intermetallic compounds. To this end, the $CuGa_2$ and $NiGa_4$ (active A = Ga, inactive B = Cu and Ni) have been selected, and their electrochemical, microscopic, and structural analyses have been made. In order to locate the role of inactive B, the studies on pure Ga electrode (B-component-free) were made in parallel and property differences to that of intermetallic compounds were monitored.

Experimental Section

Preparation. The electrode samples were prepared in different ways according to the targeted experiments. For the electrochemical characterization, ex-situ X-ray diffraction (XRD) analysis, and Raman study, the pure Ga and $CuGa_2$ electrodes were prepared as a thick film (ca. 6 μm). For the Ga electrode, liquid Ga (melting point = 29.8 °C) was spread on a piece of Mo foil (thickness = 25 μm) using a slide glass. For the $CuGa_2$ electrode, however, liquid Ga was spread on a piece of Cu foil (thickness = 25 μm) and heated at 120 °C for 12 h under vacuum. Even if the $CuGa_2$ intermetallic formation is possible at ambient temperature, the 120 °C treatment was made to complete the reaction. For the in-situ XRD analysis, the foil current collector was replaced with Mo and Cu mesh because, with the foil current collector, the electrode layer was not easily accessed by the electrolyte solution due to a very narrow gap between the electrode and beryllium window in the electrochemical XRD cell. With the meshes, however, the electrolyte solution can be easily penetrated into the electrode layer through the holes. The samples for TEM analysis were prepared as a powder form and formulated as a composite electrode. To this end, a few tens of micrometers sized $CuGa_2$ powder was prepared by mixing metallic Cu and liquid Ga in mortar and subsequent heating at 120 °C for 12 h under vacuum. The composite electrode was prepared by spreading a slurry mixture of $CuGa_2$ powder, poly(vinylidene fluoride) (PVDF, as a binder), and super P (as a carbon additive for conductivity enhancement) (10:1:1.5 in weight ratio) on a piece of Cu foil or Mo mesh. All chemicals were purchased from Aldrich.

Characterization of Materials. For the in-situ XRD analysis, a specially designed electrochemical cell with beryllium window was mounted on a D8-Brucker diffractometer equipped with Cu Kα radiation (1.540 56 Å). For the ex-situ XRD analysis, cells were disassembled and electrodes were washed with dimethyl carbonate (DMC) and dried in an Ar-filled drybox. All the XRD patterns were recorded at 3 kV and 30 mA using continuous scanning mode with 0.75° min^{-1}. The Raman study was made with a LabRam HR (Jobin-Yvon Co., France) spectrometer with a 632.8 nm He/Ne laser operating at 0.62 mW. Signals were collected by using a multichannel charge-coupled device (CCD) detector cooled to 140 K. The field emission-scanning electron microscopy (FE-SEM) analysis was made with a JEOL JSM-6700F, whereas the transmission electron microscopy (TEM) and annular dark-field scanning transmission electron microscopy (ADF-STEM) images, energy dispersive spectroscopy (EDS) elemental mapping, and selected area diffraction (SAD) patterns were obtained using a JEOL JEM-3000F at 300 kV acceleration voltage.

Electrochemical Characterization. Cells were assembled in an Ar-filled glovebox and tested in a temperature-controlled oven. The galvanostatic charge–discharge cycling was made with a two-electrode 2032-type coin cell in the potential range of 0.0–2.0 V (vs Li/Li^+). Li metal foil was used as the counter electrode. Different electrolytes were used according to the test temperatures: 1.0 M $LiPF_6$ dissolved in a mixture of ethylene carbonate (EC) and dimethyl carbonate (DMC) (1:1 v/v) at ≤55 °C and 1.0 M lithium bis(perfluoroethylsulfonyl)imide (LiBETI) in propylene carbonate (PC) or 1.0 M lithium bis(oxalate)borate (LiBOB) in a mixture of ethylene carbonate (EC) and diethyl carbonate (DEC) (1:1 v/v) at ≥85 °C. As the separator, porous polypropylene (PP) film was used for the test at ≤55 °C but a glass fiber sheet at ≥85 °C since PP separator is deformed at ≥85 °C.

Results and Discussion

In order to see how the inactive component (Cu) affects the thermodynamic properties of active component (Ga) in $CuGa_2$ intermetallic compound, the quasi-equilibrium voltage−composition profiles of $CuGa_2$ electrode were traced by the galvanostatic intermittent titration technique (GITT) at 120 °C and presented Figure 1a along with the results obtained with the Cu-free electrode (pure Ga). Note that this experiment was made to identify the phase evolution associated with Li^+ uptake/extraction for $CuGa_2$ electrode, but the measurement was made at 120 °C because the available composition range (x in Li_xGa) is limited at 25 °C due to large polarization, as shown in Figure 1b. Furthermore, even if the voltage−composition profile of pure Ga electrode can be obtained at 25 °C, the 120 °C profile is provided in Figure 1a to compare the thermodynamic property of two systems at the same temperature. As seen in Figure 1a, the pure Ga electrode shows largely the same quasi-equilibrium voltage profiles on lithiation (circles) and delithiation (triangles). Four consecutive voltage plateaus illustrate that four different two-phase reactions are involved. From the x values in Li_xGa, the lithiated Ga phases can be identified as those indicated at the top of Figure 1a. Further, the ex-situ XRD analysis

(15) Kepler, K. D.; Vaughey, J. T.; Thackeray, M. M. *Electrochem. Solid-State Lett.* **1999**, *2*, 307.
(16) Larcher, D.; Beaulieu, L. Y.; MacNeil, D. D.; Dahn, J. R. *J. Electrochem. Soc.* **2000**, *147*, 1658.
(17) Dahn, J. R.; Mar, R. E.; Abouzeid, A. *J. Electrochem. Soc.* **2006**, *153*, A361.
(18) Mukaibo, H.; Sumi, T.; Yokoshima, T.; Momma, T.; Osaka, T. *Electrochem. Solid-State Lett.* **2003**, *6*, A218.
(19) Tarascon, J. M.; Morcrette, M.; Dupont, L.; Chabre, Y.; Payen, C.; Larcher, D.; Pralong, V. *J. Electrochem. Soc.* **2003**, *150*, A732.
(20) Song, S. W.; Reade, R. P.; Cairns, E. J.; Vaughey, J. T.; Thackeray, M. M.; Striebel, K. A. *J. Electrochem. Soc.* **2004**, *151*, A1012.
(21) Larcher, D.; Beaulieu, L. Y.; Mao, O.; George, A. E.; Dahn, J. R. *J. Electrochem. Soc.* **2000**, *147*, 1703.
(22) Fleischauer, M. D.; Obrovac, M. N.; McGraw, J. D.; Dunlap, R. A.; Topple, J. M.; Dahn, J. R. *J. Electrochem. Soc.* **2006**, *153*, A484.
(23) Fehlner, F. P.; Mott, N. F. *Oxid. Met.* **1970**, *2*, 59.

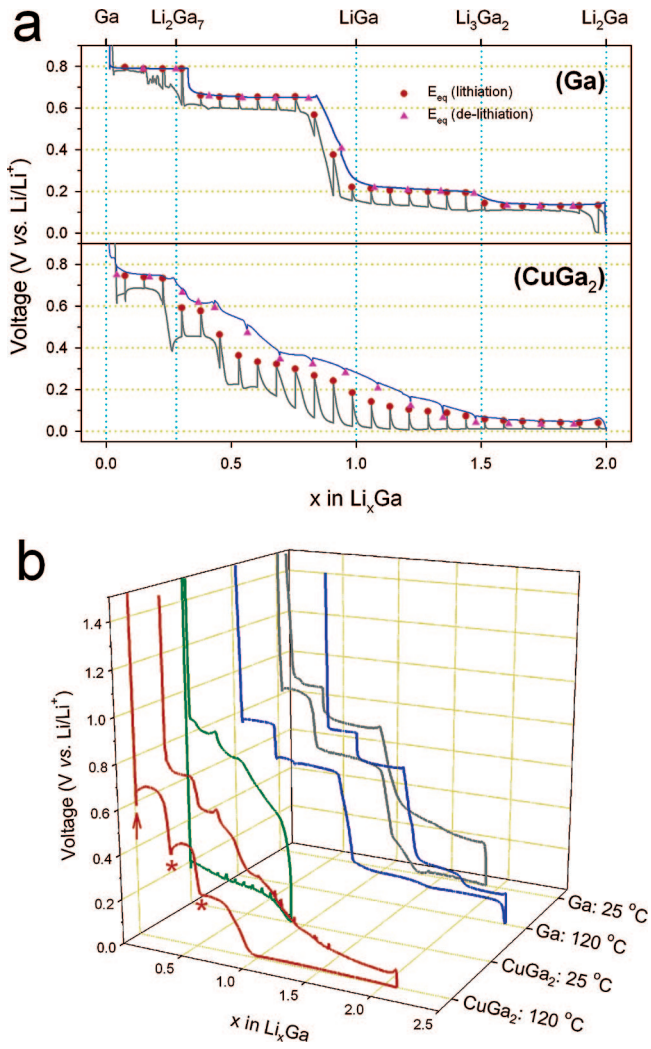

Figure 1. (a) Quasi-equilibrium voltage−composition profiles (E_{eq}) of pure Ga and $CuGa_2$ electrode that were traced by the galvanostatic intermittent titration technique (GITT) at 120 °C. For each step, a specific current of 5 mA g_{Ga}^{-1} was applied for 5 h and then rested for 10 h to reach a quasi-equilibrium voltage. The profiles are normalized by the theoretical capacity of Li_2Ga. (b) Galvanostatic lithiation/delithiation voltage profiles traced at 25 and 120 °C for two electrodes (specific current = 10 mA g_{Ga}^{-1}).

(Figure 2a) confirmed the presence of these intermediate Li−Ga phases, from which the following lithiation (the right direction) and delithiation (the left direction) pathways are identified:[24,25]

$$Ga \leftrightarrow Li_2Ga_7 \leftrightarrow LiGa \leftrightarrow Li_3Ga_2 \leftrightarrow Li_2Ga$$

In this electrode, one Ga atom is lithiated with up to two Li atoms (Li_2Ga, theoretical specific capacity = 769 mA h g_{Ga}^{-1}) and the original metallic Ga is restored at the end of delithiation. The Ga-containing binary intermetallic compound, $CuGa_2$, shows a similar but apparently different voltage−composition profile to that of pure Ga (Figure 1a): It is also lithiated up to Li_2Ga and recovered to pure Ga after delithiation. The $CuGa_2$ electrode, however, differs from pure Ga in several aspects on its voltage−composition profile (Figure 1a). First, the four voltage plateaus are now difficult to be distinguished. Second, the ex-situ XRD analysis (Figure 2b) indicates that the Li_xGa phases evolved during lithiation are somewhat different to those appeared on delithiation:

on lithiation: $CuGa_2 \rightarrow$ unknown/Cu $\rightarrow$ LiGa/Cu $\rightarrow$ Li_2Ga/Cu

on delithiation: Li_2Ga/Cu $\rightarrow$ LiGa/Cu $\rightarrow$ Li_2Ga_7/Cu $\rightarrow$ (Ga/Cu) $\rightarrow$ $CuGa_2$

Even further, the Li_3Ga_2 phase that appears in pure Ga electrode is now missing. Given the fact that metallic Cu is generated in the $CuGa_2$ electrode at the beginning of lithiation and remains as an elemental state until it combines with metallic Ga that is restored at the final stage of delithiation (Figure 2b), it is not difficult to assume that the unexpected thermodynamic behavior (phase evolution in the binary Li−Ga system) for $CuGa_2$ electrode is associated with the presence of metallic Cu. That is, the metallic Cu is not idling; rather, it exerts a strong influence on the thermodynamic properties of the lithiated Ga phases (Li_xGa). The discussion on this issue will be advanced in the later section.

The kinetic properties of $CuGa_2$ electrode is also influenced by the presence of metallic Cu as evidenced by the variable-temperature galvanostatic (thus, transient) lithiation/delithiation voltage profiles. As shown in Figure 1b, the pure Ga electrode is lithiated/delithiated with four plateaus at 25 and 120 °C even if some plateaus are shorter or longer than the theoretical capacities (Figure 1a) due to irreversible electrolyte decomposition or detachment of Ga component from Mo foil due to poor adhesion between two layers. The $CuGa_2$ electrode also takes up and extracts two Li per Ga at 120 °C with a voltage profile similar to the quasi-equilibrium voltage−composition profile. The transient profile, however, gives a revealing feature that a dip appeared at the commencement of lithiation (marked with arrow). In general, such a dip appears when electrode reaction requires a formation of new phase but disappears once large enough nuclei are generated.[26] For instance, a dip is observed in the discharge curve of Zn−HgO cells, where activation energy is needed for bond cleavage and Hg nuclei formation at the HgO cathode.[26] Along this line, the dip appeared in this work can be ascribed to the activation energy needed for bond cleavage between Cu and Ga and phase formation of metallic Cu and Li_xGa. The larger electrode polarization (the difference between the transient and quasi-equilibrium voltage) than that for pure Ga for the first plateau further supports the nucleation overpotential that is associated with bond dissociation and nuclei formation. Further, the incomplete lithiation (only up to LiGa) observed with the $CuGa_2$ electrode at 25 °C can thus be accounted for by the electrode polarization.

Another interesting observation made in Figure 1b is that the dips appear at the starting point of each two-phase reaction (most apparently, at the beginning of the second and third plateau as marked with *), and the electrode polarization still remains larger than that for pure Ga

(24) Saint, J.; Morcrette, M.; Larcher, D.; Tarascon, J. M. *Solid State Ionics* **2005**, *176*, 189.
(25) Wen, C. J.; Huggins, R. A. *J. Electrochem. Soc.* **1981**, *128*, 1636.
(26) Pletcher, D.; Walsh, F. C. *Industrial Electrochemistry*, 2nd ed.; Chapman and Hall: London, 1990; pp 546–549.

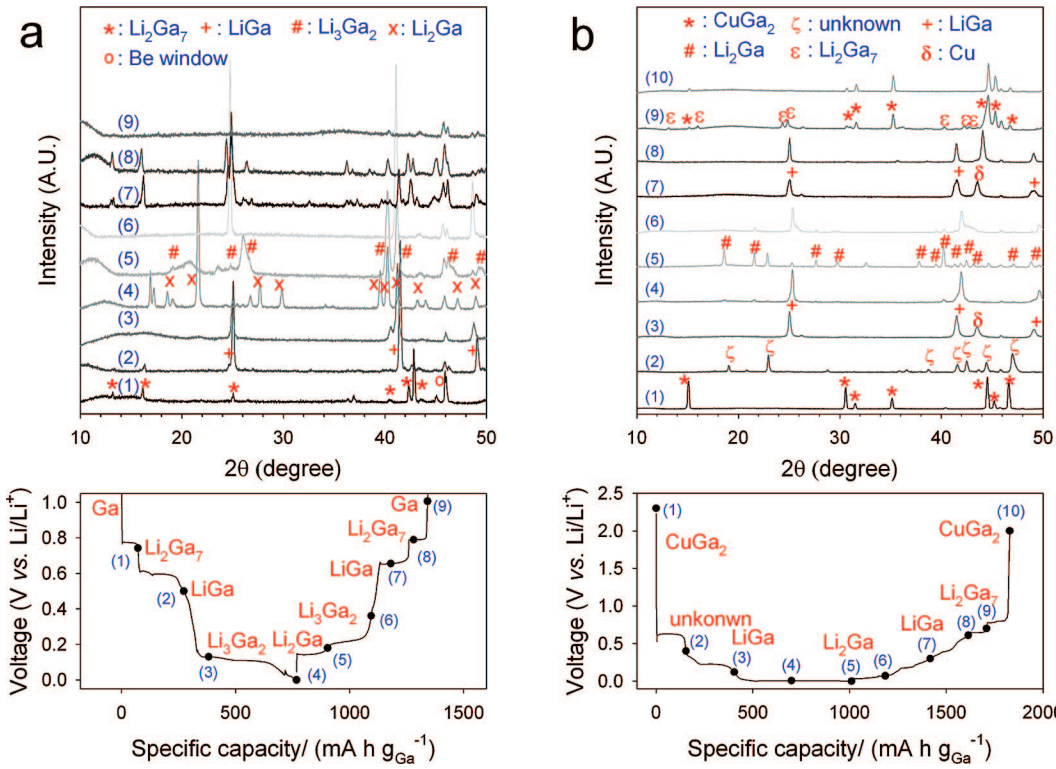

Figure 2. Ex-situ XRD patterns and voltage profiles recorded with (a) Ga electrode and (b) $CuGa_2$ electrode (temperature = 120 °C and specific current = 100 mA g_{Ga}^{-1}). The numbers denote the positions at which the XRD patterns were taken.

electrode for the whole period of lithiation. This means that another type of activation energy is required for the lithiation of intermediate Li_xGa phases, which is certainly not for the cleavage of Cu−Ga bond in $CuGa_2$ since metallic Cu and Li_xGa have already been extracted out at the beginning of lithiation. Along this line, we now propose a partial bonding between Cu and Ga atoms in Li_xGa phases.[27–30] If this phenomenon is indeed occurring, an activation energy needed for the cleavage of this partial bonding and new phase formation is required for the lithiation of intermediate Li_xGa phases. It is worthwhile to mention here that metallic Ga and Cu have such a strong affinity to each other that they easily form intermetallic compounds (for instance, $CuGa_2$ in this work) even at ambient temperature; thereby, the premise for partial bonding between Cu and Ga atoms in Li_xGa phases seems not far from real.

An unexpected electrochemical activity for the formation/decomposition of Li_2O has been reported by Poizot et al., who claimed that the reversible reaction ($MO + 2Li^+ + 2e = M + Li_2O$, where M = Co, Ni, Fe, and Cu), which is not possible with bulkier materials, is greatly facilitated since the electrochemically driven M and Li_2O carry a nanosized domain structure with extensive contact area between them.[31,32] Certainly, the partial bonding proposed in this work is only prevailing when the contact area between the Cu and Li_xGa phase is extensive and their particle size is extremely small, which is the case in this work. Figure 3a displays the bright-field TEM image taken with the sample that is lithiated up to LiGa from the $CuGa_2$ electrode, where a few tens of nanometers sized grains can be recognized. The selected area diffraction (SAD) pattern (Figure 3b) illustrates that the grains correspond to two separate polycrystalline LiGa and Cu phases that are mixed together within a few hundred nanometers scale (aperture size: ca. 250 nm). The dark-field TEM image (Figure 3c), which is obtained by using the LiGa (111) reflection that is indicated as the circle in the SAD pattern, reveals that the size of LiGa grain is less than 50 nm. The presence of nanosized Cu and LiGa grains and their even distribution were further ascertained by the annular dark-field scanning electron microscopy (ADF-STEM) and energy dispersive spectroscopy (EDS) mapping (Figure 3d). This result confirms the formation of nanosized grains and extended contact area made between two; thereby, the premise of partial bonding seems prevailing.

Evidencing results for the partial bonding are collected in Figure 4. Figure 4a compares the Raman spectra of the LiGa phase that is prepared by lithiating the pure Ga and $CuGa_2$ electrode. By the factor group analysis, totally irreducible representation for the lattice vibrations of LiGa (cubic, space group = *Fd3m*) is derived as $T_{1u}(IR) + 2T_{2g}(R)$. The Raman-active T_{2g} vibration is represented in Figure 4a. The LiGa phase derived from pure Ga gives the T_{2g} vibration at 185 cm^{-1}. A red-shift by ca. 20 cm^{-1} is, however, observed with the LiGa phase derived from $CuGa_2$ electrode, indicative of a weakening in the Li−Ga bond strength in the latter

(27) Duscher, G.; Chisholm, M. F.; Alber, U.; Rühle, M. *Nat. Mater.* **2004**, *3*, 621.
(28) Yamaguchi, M.; Shiga, M.; Kaburaki, H. *Science* **1997**, *307*, 393.
(29) Nakagawa, N.; Hwang, H. Y.; Muller, D. A. *Nat. Mater.* **2006**, *5*, 204.
(30) Ohtomo, A.; Hwang, H. Y. *Nature (London)* **2004**, *427*, 423.
(31) Poizot, P.; Laruelle, S.; Grugeon, S.; Dupont, L.; Tarascon, J. M. *Nature (London)* **2000**, *407*, 496.
(32) Thackeray, M. M.; Baker, S. D.; Adendorff, K. T.; Goodenough, J. B. *Solid State Ionics* **1985**, *17*, 175.

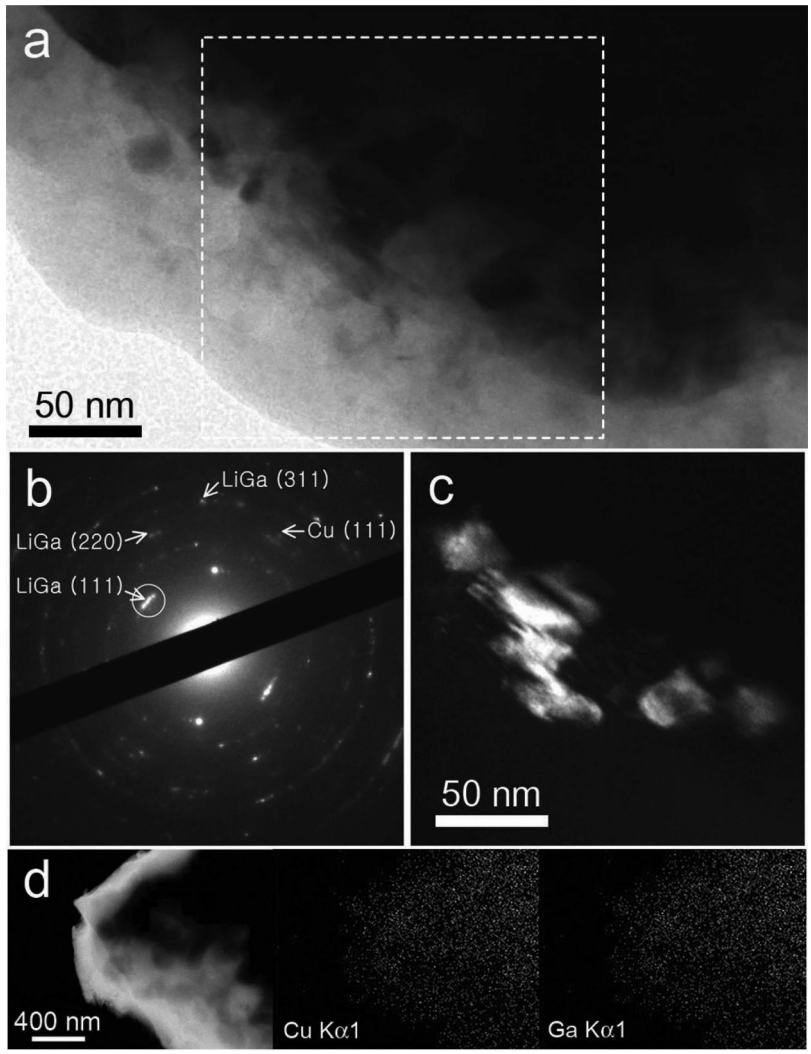

Figure 3. TEM images taken with the LiGa and Cu nanograins that were obtained from the $CuGa_2$ electrode. (a) Bright-field image. The dotted rectangle corresponds to the area for the dark-field image (c). (b) SAD pattern. The circle on LiGa (111) reflection indicates the aperture position used to take the dark-field image. (c) Dark-field image. (d) ADF-STEM image and elemental mapping showing the local EDS signals of Cu and Ga. The sample was prepared by lithiating the $CuGa_2$ electrode down to 0.0 V (vs Li/Li^+) (temperature = 55 °C and specific current = 100 mA g_{Ga}^{-1}).

sample.[3,33,34] This can be accounted for by Li−Ga←Cu bond formation, where the Li−Ga bond is weakened due to the partial bonding of Ga←Cu. The second evidencing feature for partial bonding can be found in the XRD results made on the LiGa phase. Figure 4b compares the XRD patterns recorded with the LiGa phase derived from two electrodes. One apparent feature here is the peak shift to the higher angle for (220) diffraction as compared to that for cubic LiGa phase, indicative of a lattice distortion. Lattice parameters were calculated by a peak fitting using MDI JADE 7 program. Lattice constants for the LiGa phase derived from pure Ga were calculated to be 6.13 Å (mean value of 6.135, 6.139, and 6.139 for (111), (220), and (311) planes, respectively). The insignificant deviation from the mean value indicates that this LiGa phase is cubic. A cubic setting for the LiGa phase derived from $CuGa_2$, however, results in a considerable deviation: 6.125, 6.100, and 6.144 Å for (111), (220), and (311) planes, respectively. A best fitting was achieved with orthorhombic setting: $a = 6.152$ Å, $b = 6.050$ Å, and $c = 6.175$ Å. The appreciable lattice distortion from cubic for the LiGa phase derived from $CuGa_2$ electrode illustrates that the Li−Ga bond distance in this LiGa phase differs to that for the Ga-derived LiGa (cubic lattice), presumably longer in the former since the Li−Ga bond strength is weaker as the Raman data suggest. The final evidence for partial bonding can be found in the *d*-spacing values of LiGa phase (Figure 4c) that were obtained from in-situ XRD analysis made on the $CuGa_2$ electrodes at 120 °C (Figure S1). Upon delithiation from Li_2Ga to Li_2Ga_7 through LiGa phase, the *d* spacing for (111), (220), and (311) diffraction shows a steady value in the initial period, then a gradual increase at $x = 1.3$–0.9 for Li_xGa, and finally a steady value. This illustrates that the delithiation is propagated by an initial two-phase reaction, then one-phase reaction, and another two-phase reaction, which is contrasted by the pure Ga electrode that is delithiated by the consecutive two-phase reactions (Figure 1a). The different delithiation pathway to that of pure Ga electrode, which is presented here and in the quasi-equilibrium voltage−composition profiles in Figure

(33) Inaba, M.; Iriyama, Y.; Ogumi, Z.; Todzuka, Y.; Tasaka, A. *J. Raman Spectrosc.* **1997**, *28*, 613.
(34) Julien, C.; Massot, M. *Solid State Ionics* **2002**, *148*, 53.

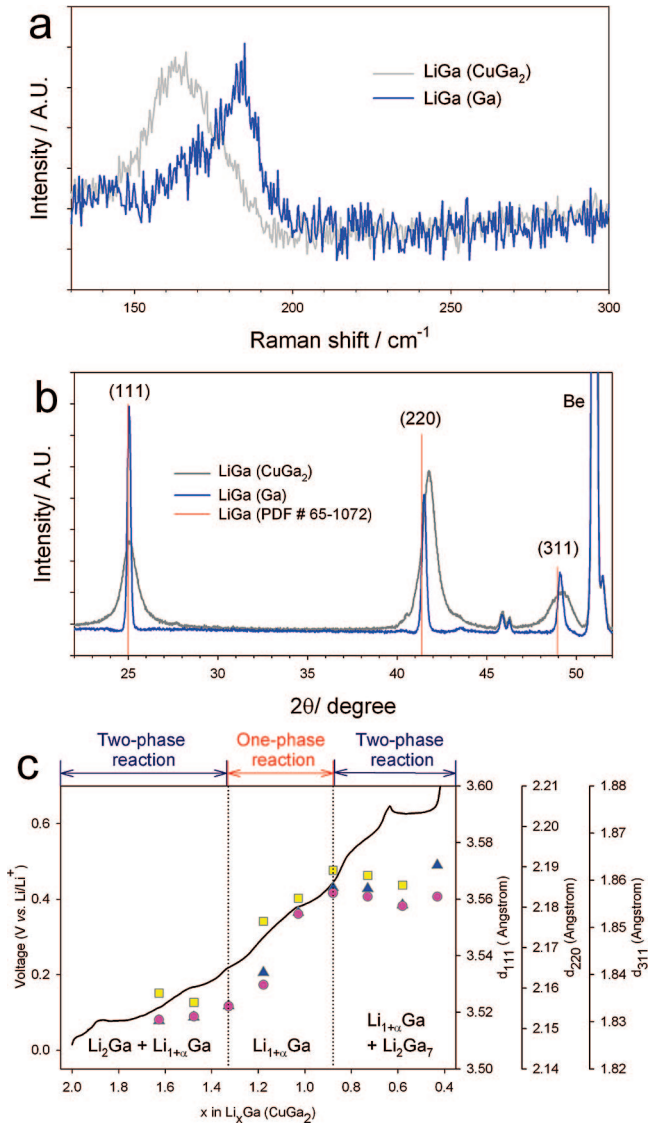

Figure 4. (a) Raman spectra taken on the LiGa phase derived from Ga and $CuGa_2$ electrodes. (b) Ex-situ XRD patterns of LiGa phase. The samples for Raman and ex-situ XRD analysis were prepared by lithiating the $CuGa_2$ and Ga electrode down to 0.0 V (vs Li/Li^+) (temperature = 25 °C and specific current = 10 mA g_{Ga}^{-1}). (c) *d*-spacing values of LiGa phase derived from the $CuGa_2$ electrode (temperature = 120 °C). The triangles, circles, and squares denote the d_{111}, d_{220}, and d_{311}, respectively.

1a, should thus be explained by the strong influence exerted by the extracted Cu.

In theory, unusual thermodynamic properties can be assumed with nanosized materials since they carry such a large surface-to-volume ratio that the surface energy is the more influencing factor than internal energy in controlling the thermodynamics of systems.[35] In real, several reports have already demonstrated the size-dependent thermodynamic properties in nanosized materials.[1,3,19,36–41] For instance, Wagemaker and co-workers reported that the phase

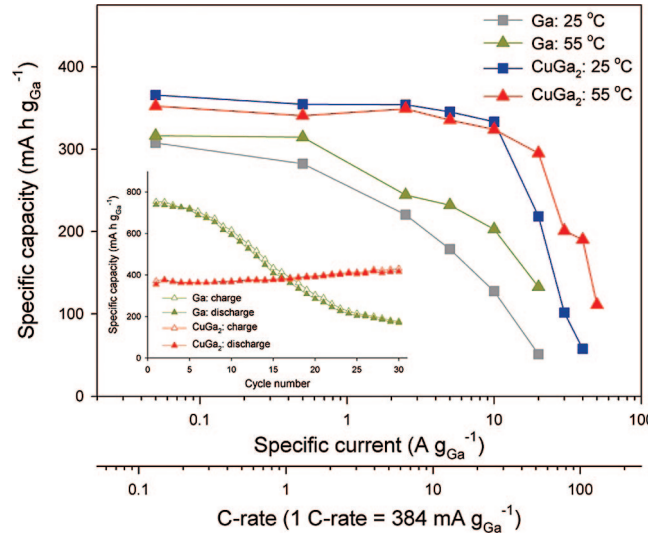

Figure 5. Delithiation rate performance of Ga and $CuGa_2$ electrodes (0.0–2.0 V vs Li/Li^+). The electrodes were lithiated up to LiGa phase to compare their delithiation rate performance from LiGa to pure Ga. Note that the lithiation condition differs at two temperatures: The $CuGa_2$ electrodes were lithiated to 0.0 V (vs Li/Li^+) with a specific current of 10 and 100 mA g_{Ga}^{-1} at 25 and 55 °C, respectively. The Ga electrodes were lithiated to 0.0 and 0.1 V (vs Li/Li^+) with a specific current of 100 mA g_{Ga}^{-1} at 25 and 55 °C, respectively. Cycle performance is also compared for Ga and $CuGa_2$ electrode in the inset (temperature = 55 °C and specific current = 100 mA g_{Ga}^{-1}).

diagram of $Li-TiO_2$ (anatase) alters significantly according to the particle size of TiO_2.[36] This observation has been ascribed to the phase boundary energetics that plays an important role in determining the thermodynamic properties even when the particle size is as large as 40 nm. As an example in other disciplines, Murakoshi and co-workers reported unusual phase transitions and formation of metastable phases in ZnS nanocrystallites that were induced by surface covalent or ionic bonding by adsorbates.[37] The authors verified the formation of chemical bonds between surface Zn atoms of ZnS nanocrystallites and organic anions, from which the unexpected thermodynamic behavior has been ascribed to a change in the surface energy of ZnS nanocrystallites upon a surface chemical bonding. When account is taken of the importance of surface energy claimed in several nanosystems, the unusual thermodynamic properties observed in this work, the different phase evolution in $CuGa_2$ to that for pure Ga, can now be explained by an alteration in the surface energy of Li_xGa nanograins, which is in turn caused by extracted metallic Cu through partial bonding.

Figure 5 compares the delithiation rate capability for two electrodes, which was derived from the galvanostatic charge–discharge voltage profiles provided in the Supporting Information (Figure S2). Both electrodes were lithiated up to LiGa phase (theoretical capacity = 384 mA h g_{Ga}^{-1}) and delithiated with specific currents ranging from 50 mA g_{Ga}^{-1} (0.13 *C*) to 50 A g_{Ga}^{-1} (130 *C*). For this work, film electrodes having a similar thickness (ca. 6 μm) were used to exclude

(35) Maier, J. *Nat. Mater.* **2005**, *4*, 805.
(36) Wagemaker, M.; Borghols, W. J. H.; Mulder, F. M. *J. Am. Chem. Soc.* **2007**, *129*, 4323.
(37) Murakoshi, K.; Hosokawa, H.; Tanaka, N.; Saito, M.; Wada, Y.; Sakada, T.; Mori, H.; Yanagida, S. *Chem. Commun.* **1998**, 321.
(38) Meethong, N.; Huang, H. Y. S.; Carter, W. C.; Chiang, Y. M. *Electrochem. Solid-State Lett.* **2007**, *10*, A314.
(39) Kavan, L.; Kalbac, M.; Zukalova, M.; Exnar, I.; Lorenzen, V.; Nesper, R.; Graetzel, M. *Chem. Mater.* **2004**, *16*, 477.
(40) Kavan, L.; Prochazka, J.; Spitler, T. M.; Kalbac, M.; Zukalova, M.; Drezen, T.; Graetzel, M. *J. Electrochem. Soc.* **2003**, *150*, A1000.
(41) Sudant, G.; Baudrin, E.; Larcher, D.; Tarascon, J. M. *J. Mater. Chem.* **2005**, *15*, 1263.

any thickness effect (for instance, Li^+ diffusion length). The electrode–film thickness was 5.98 ± 0.44 μm for Ga at 25 °C, 6.21 ± 0.60 μm for Ga at 55 °C, 5.83 ± 0.19 μm for $CuGa_2$ at 25 °C, and 5.67 ± 0.54 μm for $CuGa_2$ at 55 °C. The electrode thickness was calculated on the basis of the weight of Ga, apparent area of electrode, and specific density of Ga and $CuGa_2$ and was confirmed by the FE-SEM analysis (Figure S3). The $CuGa_2$ electrode shows a much higher delithiation rate as compared to that for pure Ga: at 25 °C, the specific capacity is 366 mA h g_{Ga}^{-1} at 0.13 *C* and 333 mA h g_{Ga}^{-1} at 26.0 *C*. It is surprising that the delithiation rate capability of $CuGa_2$ electrode is as good as those reported for nanosized electrode materials[1–9] or supercapacitors.[42,43] The unusually high delithiation rate can be accounted for by the partial bonding proposed in this work. As a result of Cu → Ga partial bonding, the Ga−Li bond is weakened to allow a facilitated delithiation reaction. Unexpected kinetic properties in nanosized electrode materials have also been reported by Meethong and co-workers, who demonstrated that the rate capability of $LiFePO_4$ is improved owing to a minimized lattice misfit between coexisting phases when the particle size is reduced by nanoscaling.[44] It is thus very likely that unusual kinetics is further found in the future work with other nanosized electrode systems even if the underlying mechanism for the enhancement of rate capability differs from one system to another (for instance, partial bonding for $CuGa_2$ in this work and reduced misfit for $LiFePO_4$). The cycle performance of two electrodes is compared in the inset of Figure 5. At 55 °C, the pure Ga electrode delivers a first lithiation capacity amounting to its theoretical value (769 mA h g_{Ga}^{-1}) as it is fully lithiated up to two Li atoms per Ga (Li_2Ga), whereas the first lithiation capacity of $CuGa_2$ electrode amounts to 380 mA h g_{Ga}^{-1} because the lithiation is possible only to one Li atom per Ga (LiGa) due to electrode polarization. The $CuGa_2$ electrode, however, shows a better cycle performance as compared to the pure Ga without significant capacity loss with cycling. Also, the first irreversible capacity for two electrodes is very small: the Coulombic efficiency of $CuGa_2$ and Ga electrode in the first cycle is 95.6% and 98.0%, respectively. It is likely that electrolyte decomposition is insignificant as the surface exposed to electrolyte solution is small in these film electrodes.

A similar observation has been made with another Ga-containing binary intermetallic compound ($NiGa_4$). As shown in the Supporting Information, the $NiGa_4$ electrode also shows a different thermodynamic behavior (voltage−composition profile) to that of pure Ga as evidenced by the ex-situ XRD analysis (Figure S4). On aspect of kinetics, the lithiation rate of $NiGa_4$ electrode is slower due to activation energy needed for the cleavage of Ni−Ga bond (Figure S5), but the delithiation rate is higher than the pure Ga electrode (Figure S6). Now, a question arises as to whether the role of inactive component unraveled in this work is also effective in other binary intermetallic compounds (A_xB_y, where A = Si, Sn, and Sb, and B = Cu, Ni, or other metallic elements). If this is the case, a tradeoff between lithiation and delithiation rate seems to be possible by a deliberate selection of active A and inactive B component. For instance, if the affinity and thereby bond strength between two are intermediate, negative electrode materials delivering a reasonable rate at both charge and discharge can be derived. This work is now underway in this laboratory.

Conclusion

In this paper, the role of inactive component (Cu and Ni) affecting the thermodynamic and kinetic properties of active component (Ga) in binary intermetallic electrodes ($CuGa_2$ and $NiGa_4$) is highlighted. The following points are summarized: (i) The variable temperature (25–120 °C) electrochemical study indicates that the binary intermetallic electrodes show a slower lithiation kinetics than the pure Ga electrode due to the bond cleavage and new phase formation. (ii) The microscopic study reveals a formation of nanograins of Cu and lithiated Ga upon lithiation. (iii)On the basis of Raman and XRD results, a partial bonding between two electrochemically driven nanograins has been proposed. On the basis of this interfacial phenomenon, the unexpected thermodynamic properties (quasi-equilibrium voltage−composition profiles) and kinetic properties (exceptionally good delithiation rates) of the binary intermetallic electrodes have been explained. These intermetallic electrodes seem applicable as the negative electrode for lithium secondary batteries that discharge at high rates. Further, the electrochemically driven nanostructure approach can be applied to other systems for the development of high-rate electrode materials.

Acknowledgment. This work was supported by KOSEF through the Research Center for Energy Conversion and Storage.

Supporting Information Available: In-situ XRD patterns made on $CuGa_2$ electrode at 120 °C, the galvanostatic delithiation voltage profiles recorded with the pure Ga and $CuGa_2$ electrodes, the cross-sectional FE-SEM image taken with $CuGa_2$ film electrode, the ex-situ XRD patterns made on $NiGa_4$ electrodes at 120 °C, the variable-temperature galvanostatic lithiation/delithiation voltage profiles traced with $NiGa_4$ electrode, and the delithiation rate performance of $NiGa_4$ electrode. This material is available free of charge via the Internet at http://pubs.acs.org.

CM702181M

(42) Kötz, R.; Carlen, M. *Electrochim. Acta* **2000**, *45*, 2483.
(43) Yoon, S.; Lee, J.; Hyeon, T.; Oh, S. M. *J. Electrochem. Soc.* **2000**, *147*, 2507.
(44) Meethong, N.; Huang, H. Y. S.; Speakman, S. A.; Carter, W. C.; Chiang, Y. M. *Adv. Funct. Mater.* **2007**, *17*, 1115.